Compressional and shear wave velocities in uncemented sediment containing gas hydrate

T. S. Yun,[1] F. M. Francisca,[1,2] J. C. Santamarina,[1] and C. Ruppel[3]

[1] The competing hypotheses for gas hydrate formation at the particle scale in sediments describe processes of pore-filling, frame-building, or cementation. New measurements of compressional (V_P) and shear wave (V_S) velocities in fine-grained sands subjected to low confinement and monitored during formation of tetrahydrofuran hydrate indicate that hydrate nucleates in the pore space (presumably at grain boundaries) and grows with limited impact on the sediment shear stiffness, V_P, and V_S until crystals begin to interact with the granular skeleton at ~40% hydrate concentration. V_S increases significantly more than V_P at higher hydrate concentrations, reflecting larger changes in the specimen's shear stiffness than its bulk stiffness. The results indicate that seismic velocities and/or their ratio (V_P/V_S) have limited capability for locating hydrate or constraining hydrate concentrations. **Citation:** Yun, T. S., F. M. Francisca, J. C. Santamarina, and C. Ruppel (2005), Compressional and shear wave velocities in uncemented sediment containing gas hydrate, *Geophys. Res. Lett.*, *32*, L10609, doi:10.1029/2005GL022607.

1. Introduction

[2] Natural gas hydrate deposits are often studied using seismic methods that detect features known to promote hydrate formation (e.g., permeable layers, faults) and that sometimes constrain the existence and distribution of gas hydrate and free gas. Interpretation of seismic data requires assumptions about material properties [*Lee and Collett*, 2001; *Lee*, 2002] and an understanding of microscale processes that accompany hydrate formation.

[3] The literature on microscale processes in hydrate formation has highlighted the controversy among alternative hypotheses [see *Winters et al.*, 2004]: (1) Pore filling, in which hydrate forms within the pore fluid, a process that primarily alters sediment bulk stiffness; (2) Frame-building, in which hydrate connects sediment grains and contributes to the sediment's rigidity; and (3) Cementation, in which hydrate growth initiates around particles, including at interparticle contacts. The last two processes affect both the sediment's shear stiffness and bulk stiffness.

[4] Studies designed to determine how hydrate forms in porous sediments have produced equivocal results.

Using effective media approaches, *Dvorkin and Nur* [1983] and *Dvorkin et al.* [2000] concluded that hydrate principally modifies the skeletal properties of porous media, consistent with hydrate growing at grain contacts (cementation). Field-scale seismic data [*Ecker et al.*, 1998; *Helgerud et al.*, 1999] appear to substantiate this result. In contrast, laboratory measurements [*Kunerth et al.*, 2000] of compressional wave (P-wave; V_P) and shear wave (S-wave; V_S) velocities in hydrate-bearing sands imply that hydrate formation primarily affects the bulk stiffness of sediments, a result consistent with the pore filling hypothesis.

[5] In this paper, we describe new experimental results that clarify the microscale processes accompanying hydrate formation in porous media and provide guidelines for the extrapolation of laboratory results to field settings.

2. Experimental Method

[6] Our experiments were designed specifically to study particle-level processes associated with hydrate formation in porous media. Experiments were conducted in a cylindrical cell (57.3 mm in diameter and 30 mm high). The fine-grained sand specimens (grain size 120 μm, specific surface 0.019 m^2 g^{-1}, and average porosity 0.37) were constrained at a very low mean effective stress (<10 kPa), a condition inferred from velocity-stress data acquired in calibration tests. The low effective stress state ensured that cementation-related changes in the shear stiffness of the granular skeleton were maximized during hydrate formation.

[7] The fraction of pore space filled with THF-hydrate (S_{hyd}) was controlled by varying the composition of the water-THF solution used to saturate the specimens: THF·17H$_2$O (S_{hyd} = 100% filled porosity), THF·18.2H$_2$O (95%), THF·19.5H$_2$O (89%), THF·24.6H$_2$O (74%), THF·26.8H$_2$O (69%), THF·32.4H$_2$O (58%), THF·46H$_2$O (43%) and pure water (S_{hyd} = 0%). The choice of THF as the hydrate-former for these experiments has important advantages. First, THF hydrate has similar thermomechanical properties to and the same molecular structure (Structure II) as hydrates of most thermogenic gases. Second, since THF is completely miscible in water, hydrate formation is not diffusion controlled as in the case of methane. Finally, with THF hydrate there are no complicating effects associated with free gas generation, nor must we rely on percolating the gaseous phase through the specimen to form hydrate. The latter procedure leads to preferential and predictable methane hydrate growth at water menisci [*Waite et al.*, 2004; *Priest et al.*, 2005].

[8] To minimize THF evaporation, the cell, sand, and aqueous THF solution were cooled to 6.5°C before

---

[1]School of Civil and Environmental Engineering, Georgia Institute of Technology, Atlanta, Georgia, USA.
[2]Now at Facultad de Ingenieria, Universidad Nacional de Cordoba (CONICET), Córdoba, Argentina.
[3]School of Earth and Atmospheric Sciences, Georgia Institute of Technology, Atlanta, Georgia, USA.
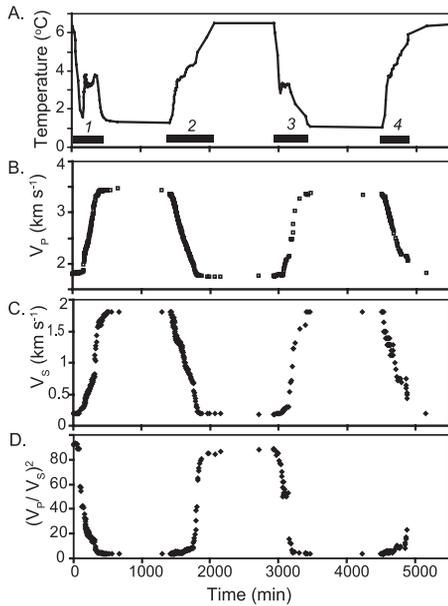
Figure 1. (a) Temperature, (b) P-wave velocity, (c) S-wave velocity, and (d) $(V_P/V_S)^2$ during hydrate formation (periods 1 and 3) and dissociation (periods 2 and 4) in a fine-grained sand specimen saturated with THF·17H$_2$O. The temperature increase near the beginning of periods 1 and 3 marks the release of exothermic heat at the onset of the hydrate phase transformation.

mixing and specimen preparation. The cell was then submerged in a cooling bath, and the temperature was gradually lowered at a rate of $\sim 1.5°C$ hr^{-1} to 0.5°C, thereby maintaining the system above the ice point for water. The temperature was controlled to a precision of 0.1°C and monitored at 4 locations, 2 inside the cell and 2 in the cooling bath. After hydrate formation was completed and the specimen temperature reached equilibrium, the water bath was warmed to 6.5°C to study dissociation processes.

[9] Elastic wave velocities were measured at 180 s intervals in transmission mode along the principal stress direction, using P-wave transducers and S-wave bender elements embedded in the top and bottom caps of the cell. The simultaneous measurements of temperature, V_P, and V_S constrained the timing of phase transformations and changes in mechanical properties.

3. Results

3.1. Phase Transformation Monitoring (Single Specimen)

[10] Figure 1 shows the evolution of internal temperature, V_P, and V_S during two cooling (hydrate formation) and warming (hydrate dissociation) cycles for a fine-grained sand specimen saturated with a THF·17H$_2$O solution. This pore fluid should undergo phase transformation at $\sim 5°C$ [*Sloan*, 1998]. However, the first hydrate formation cycle reveals supercooling to 1.6°C followed by stable phase transformation at $\sim 3.3°C$ (i.e., freezing point depression from 5°C to 3.3°C).

[11] Supercooling and freezing point depression have previously been documented for both ice and gas hydrate

systems [e.g., *Miller*, 1980; *Uchida et al.*, 2002]. The freezing point depends on the thermal characteristics of the porous medium and the concentration of THF in the pore solution. When the pore fluid has low THF concentration, the freezing point shifts towards that of water, and phase transformation proceeds more slowly and is more difficult to detect. Supercooling reflects conditions needed to promote the organization of hydrate cages and the nucleation of hydrate crystals. In the absence of mineral grains, fluids require significant supercooling to form ice (or hydrate) via homogeneous nucleation [*Miller*, 1980]. Figure 1 shows that hydrate formed more rapidly and required less supercooling during the second cooling cycle (supercooling to only 2.8°C). V_P and V_S remain constant (no phase transformation) until hydrate formation commences, coinciding with the observed increase in temperature.

[12] Figure 1 demonstrates that both V_P and V_S increase during hydrate formation. Seismic velocities are a function of the small-strain bulk modulus K, shear modulus μ, and the density ρ of the medium and are given by $V_P = \sqrt{(K + 4\mu/3)/\rho}$ and $V_S = \sqrt{\mu/\rho}$. The increase in V_S implies that phase transformation affects the sediment's shear stiffness, and the increase in V_P reflects an increase in bulk stiffness, shear stiffness, or both. To directly examine the
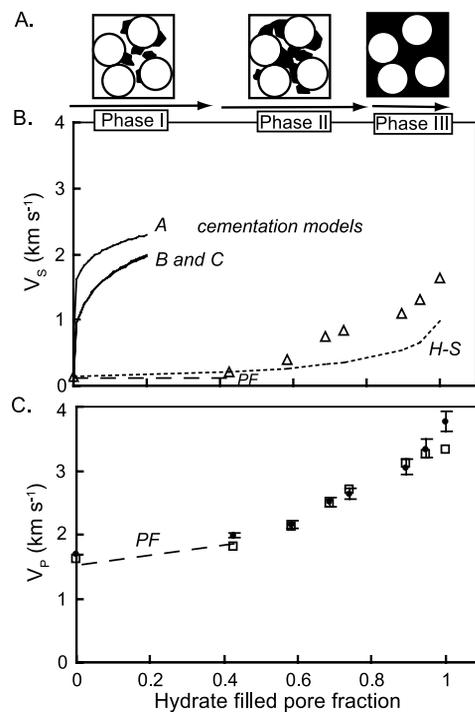
Figure 2. (a) Hydrate formation mechanism consistent with our results. (b) Measured V_S (triangles) for specimens containing finite concentrations of gas hydrate. Superposed are predicted V_S for the pore-filling model (PF-dashed line), Hashin-Shtrikman lower bound (HS-dotted line), and various cementation models: A, cementation formulation of *Ecker et al.* [1998] and B and C, loading before and after cementation, respectively [*Fernandez and Santamarina*, 2000]. (c) Measured (squares) V_P and predicted values (filled circles with error bars) based on equation (2), measured V_S, and the parameters in Table 1.

Table 1. Parameters Used in Calculation of Models (Italics) and V_P for Figure 2b and 2c, Respectively

Parameter	Value
Bulk modulus of fluid phase, K_f [GPa]	2.29
Bulk modulus of mineral grains, K_g [GPa]	36,[a, b, c] 36.6,[d] 37.8[e]
Bulk modulus of hydrates, K_{hyd} [GPa]	6.41,[a] 7.7,[b] 8.7,[d] 6.3[e], 5.6[c]
Shear modulus of mineral grains, μ_g [GPa]	45,[a, b, d, c] 44.1[e]
Shear modulus of hydrates, μ_{hyd} [GPa]	2.4[f]
Poisson's ratio of hydrates, ν_{hyd}	0.33[f]
Poisson's ratio of mineral grains, ν_g	0.15

[a]*Lee* [2002].
[b]*Chand et al.* [2004].
[c]*Ecker et al.* [1998].
[d]*Waite et al.* [2004].
[e]*Winters et al.* [2004].
[f]*Sloan* [1998].

evolution of bulk and shear stiffnesses, we plot $(V_P/V_S)^2 = K/\mu + 4/3$ in Figure 1d.

3.2. Seismic Velocities for Different Concentrations of Gas Hydrate (Multiple Specimens)

[13] Whereas the experiment described in Figure 1 focused on monitoring a single specimen during pore fluid transformation from 0% to 100% hydrate and back, Figure 2 shows V_P and V_S recorded for 8 specimens containing specific amounts of hydrate after phase transformation is completed. Therefore, these data are not biased by the non-homogeneous, time-varying hydrate distribution that may develop in the specimen used for the first experiment.

[14] Figure 2 shows that neither V_P nor V_S changes appreciably until S_{hyd} exceeds ~40%, a result that is in general agreement with field-based observations [*Guerin and Goldberg*, 2002; *Kleinberg et al.*, 2005]. We interpret the V_S data (Figure 2b) by comparing the experimental results to the predictions of microstructural models. The lowest predicted velocities correspond to the pore filling model, which produces no change in V_S until hydrate crystals contact multiple sediment grains (cementation). From geometric analyses, we calculate that spherical hydrate growths would contact neighboring particles arranged with either simple cubic or cubic tetrahedral packing when S_{hyd} reaches ~43% to 45%. Also shown is the lower bound predicted by the Hashin-Shtrikman model (frame-building model). The upper bounds in Figure 2b correspond to distinct cementation models in which hydrate coats the particles and contributes to the contact area, thus rapidly increasing the effective stiffness of the skeleton even for very low S_{hyd}.

[15] To interpret the V_P data (Figure 2c), we adopt the asymptotic form of Gassmann's equation applicable to granular materials characterized by skeletal bulk stiffness K_{sk} much smaller than the mineral grain bulk stiffness K_g. The bulk modulus of hydrate-bearing sediments K_{hbs} reflects the resistance to volumetric strain manifested by each component and involves the bulk stiffness of the skeleton K_{sk}, the fluid K_f, the hydrate K_{hyd}, and the grains K_g [*Santamarina et al.*, 2001]:

$$K_{hbs} = K_{sk} + \left[\frac{1-\phi}{K_g} + \phi \left(\frac{(1-S_{hyd})}{K_f} + \frac{S_{hyd}}{K_{hyd}} \right) \right]^{-1}, \quad (1)$$

where ϕ is sediment porosity. Combining (1) with the seismic velocities allows direct determination of V_P from V_S:

$$V_P = \sqrt{ V_S^2 \left[\frac{2(1+\nu_{sk})}{3(1-2\nu_{sk})} + \frac{4}{3} \right] + \frac{1}{\rho} \left[\frac{1-\phi}{K_g} + \phi \left(\frac{(1-S_{hyd})}{K_f} + \frac{S_{hyd}}{K_{hyd}} \right) \right]^{-1} },$$

$$(2)$$

where ν_{sk} is Poisson's ratio for the granular skeleton only. Before hydrate formation, $\nu_{sk} \cong 0.1$ to 0.2, while $\nu_{sk} \cong 0.3$ to 0.35 for $S_{hyd} = 100\%$. Figure 2c shows the range of predicted V_P values calculated from the measured V_S values based on (2) and the parameters in Table 1. These results corroborate the validity of the Biot-Gassmann model for P-waves in hydrate-bearing sediments.

4. Discussion

[16] The relative variation in bulk and shear stiffness (K/μ) with hydrate concentration is explored in Figure 3. For the time-varying data in Figure 1, the hysteresis observed in the first cooling/warming cycle decreases during subsequent cycles, probably due to residual hydrate molecular structures in the pore fluid when the specimen is warmed by only a limited amount above the hydrate dissociation temperature [*Sloan*, 1998]. Comparison of the evolving seismic velocities measured during hydrate formation for the specimen containing THF·17H$_2$O pore fluid (from Figure 1) to the seismic velocities measured for specimens with specified final hydrate concentration (from Figure 2) reveals close agreement of the datasets, corroborating our visual observations that hydrate is homogeneously distributed in all specimens.

[17] While Figure 2 demonstrates that the changes in V_S for $S_{hyd} < \sim40\%$ are too small to be consistent with the cementation model, Figure 3 implies that the skeletal shear stiffness changes enough between $S_{hyd} = 0\%$ and 43% to produce a pronounced drop in $(V_P/V_S)^2$. For low confinement experiments, this observation might be incorrectly interpreted as indicating particle cementation. In fact, the change in $(V_P/V_S)^2$ for $S_{hyd} < 43\%$ reflects the fact that hydrate can nucleate with equal probability anywhere on a grain surface adjacent to a pore. Sometimes that nucleation is close enough to a grain contact
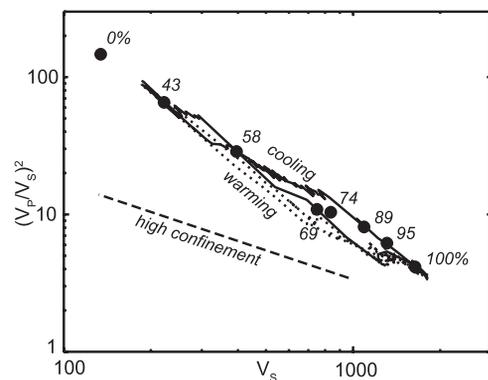
Figure 3. $(V_P/V_S)^2$ as a function of V_S for specimens with S_{hyd} as indicated (filled circles) and during phase transformation from 0% to 100% (lines). At high confinement, the slope of the curve changes as shown.

that the hydrate crystal begins to cement grains as it grows. Experiments that we have conducted at high confinement do not reveal such an apparent cementation effect at low hydrate concentrations.

[18] Figure 2a shows the evolutionary path that we infer for hydrate formation in porous media: During Phase I, hydrate nucleates in pores (presumably on mineral grains) and grows into the pore space, leading to limited increases in interparticle coordination. In Phase II, further crystal growth causes interaction among hydrate crystals, definitively increasing the effective contact number in the mineral-hydrate skeleton and producing a significant increase in skeletal shear stiffness. During Phase III, hydrate continues growing to completely fill the pore space.

[19] Our results underscore several limitations on using solely V_P, V_S, or their ratio to constrain hydrate concentrations. First, Figure 2 reveals little change in V_P and V_S until S_{hyd} exceeds 40%. Such high concentrations are generally confined to layers of highly permeable sediments within much thicker sequences, meaning that seismic surveys may reveal more about characteristics of marine sediments other than hydrate concentrations. Second, for this low effective confinement experiment, V_P nearly doubles, V_S increases ~ 9 times, and $(V_P/V_S)^2$ decreases from ~ 96 to ~ 3.5 during the hydrate formation cycle monitored in Figure 1. The large ranges of values for these parameters underscores the difficulty of relying on them to characterize hydrate concentrations in marine sediments. Third, the skeletal shear stiffness depends on effective confinement, diagenetic cementation, and hydrate concentration. The combined effect of these dependencies is such that the relative importance of hydrate-induced stiffening decreases as effective stress or diagenetic cementation increases, as is the case at depth in marine sediments [*Fernandez and Santamarina*, 2000]. This factor further complicates the interpretation of seismic velocity data in terms of hydrate concentrations.

[20] It is tempting to use (2) to predict V_S from the V_P measurements most commonly obtained in field studies, but this leads to significant errors. Defining the relative velocity error as $\varepsilon = \Delta V/V$, equation (2) yields a relationship between the relative errors ε_{V_P} and ε_{V_S} in V_P and V_S, respectively:

$$\varepsilon_{V_S} = \left[\frac{2(1 + \nu_{sk})}{3(1 - 2\nu_{sk})} + \frac{4}{3} \right]^{-1} \left[\frac{V_p}{V_s} \right]^2 \varepsilon_{V_P}, \qquad (3)$$

or simply $\varepsilon_{V_S} = \alpha\, \varepsilon_{V_P}$. The first term in brackets varies from 0.29 to 0.44 for $\nu_{sk} = 0.1$ to 0.3, while V_P/V_S ranges from >20 for saturated soft sediments to ~ 2 for cemented sediments. Thus, α ranges from ~ 1 to ~ 200. ε_{V_S} therefore has a limited effect on predictions of V_P, but ε_{V_P} will be magnified in predicting V_S. This is particularly problematic when large V_P/V_S is expected, as is the case for unconsolidated sediments subject to low confinement and having low hydrate concentration ($S_{hyd} < 40\%$).

5. Conclusions

[21] Despite the choice of experimental conditions (fine-grained sand at low confinement) that magnify the potential effects of cementation and the reliance on THF hydrate (an imperfect analog to natural methane hydrates), our results advance the understanding of the microstructure of hydrate-bearing porous media and have implications for the interpretation of seismic data collected in hydrate provinces.

[22] • At the microscale, the hydrate formation mechanism follows neither a pure cementation model nor a pure pore filling model. Experimental results suggest initial hydrate nucleation in pores (presumably at grain boundaries) followed by outward growth toward the pore space. For these sand specimens, only hydrate concentration higher than $\sim 40\%$ results in a definitive increase in skeletal shear stiffness.

[23] • The Gassmann equation can be used to predict V_P from measured V_S values. However, calculating V_S from V_P will yield unreliable results.

[24] • V_P and V_S exhibit relatively small changes when hydrate concentration increases from 0% to $\sim 40\%$. Since high concentrations of gas hydrate are not widespread in natural settings, neither V_P nor V_S alone are effective for locating gas hydrate. For most cases, we also advise caution in using V_P/V_S to infer hydrate concentrations.

References

Chand, S., T. A. Minshull, D. Gei, and J. M. Carcione (2004), Elastic velocity models for gas hydrate bearing sediments—A comparison, *Geophys. J. Int.*, 159, 573–590, doi:10.1111/j.1365-246x.2004.02387.

Dvorkin, J., and A. Nur (1983), Rock physics for characterization of gas hydrates, in *The Future of Energy Gases*, U.S. Geol. Surv. Prof. Pap., 1570, 293–298.

Dvorkin, J., M. B. Helgerud, W. F. Waite, S. H. Kirby, and A. Nur (2000), Introduction to physical properties and elasticity models, in *Natural Gas Hydrates in Oceanic and Permafrost Environments*, edited by M. Max, pp. 245–460, Springer, New York.

Ecker, C., J. Dvorkin, and A. Nur (1998), Sediments with gas hydrates: Internal structure from seismic AVO, *Geophysics*, 63, 1659–1669.

Fernandez, A., and J. C. Santamarina (2000), Effect of cementation on the small-strain parameters of sands, *Can. Geotech. J.*, 38, 191–199.

Guerin, G., and D. Goldberg (2002), Sonic waveform attenuation in gas hydrate-bearing sediments from the Mallik 2L-38 research well, Mackenzie Delta, Canada, *J. Geophys. Res.*, 107(B5), 2088, doi:10.1029/2001JB000556.

Helgerud, M. B., J. Dvorkin, and A. Nur (1999), Elastic-wave velocity in marine sediments with gas hydrates: Effective medium modeling, *Geophys. Res. Lett.*, 26, 2021–2024.

Kleinberg, R. L., C. Flaum, and T. S. Collett (2005), Magnetic resonance log of JAPEX/JNOC/GSC, Mallik 5L-38 gas hydrate production research well: Gas hydrate saturation, growth habit, and relative permeability, *Geol. Surv. Can. Bull.*, in press.

Kunerth, D. C., D. M. Weinberg, J. W. Rector, C. L. Scott, and J. T. Johnson (2000), Acoustic laboratory measurements during the formation of a THF-hydrate in unconsolidated porous media, *J. Seismic Explor.*, 9, 337–354.

Lee, M. (2002), Biot-Gassmann theory for velocities of gas hydrate-bearing sediments, *Geophysics*, 67, 1711–1719.

Lee, M., and T. Collett (2001), Elastic properties of gas hydrate-bearing sediments, *Geophysics*, 66, 763–771.

Miller, R. D. (1980), Freezing phenomena in soils, in *Application of Soil Physics*, edited by D. Hillel, pp. 254–299, Elsevier, New York.

Priest, J. A., A. I. Best, and C. R. I. Clayton (2005), A laboratory investigation into the seismic velocities of methane gas hydrate-bearing sand, *J. Geophys. Res.*, 110, B04102, doi:10.1029/2004JB003259.

Santamarina, J. C., K. A. Klein, and M. A. Fam (2001), *Soils and Waves: Particulate Materials Behavior, Characterization and Process Monitoring*, 488 pp., John Wiley, Hoboken, N. J.

Sloan, E. D. (1998), *Clathrate Hydrates of Natural Gases*, 705 pp., CRC Press, Boca Raton, Fla.

Uchida, T., I. Ikeda, S. Takeya, T. Ebinma, J. Nagao, and H. Narita (2002), CO_2 hydrate film formation at the boundary between CO_2 and water: Effect of temperature, pressure and additives, *J. Crystal Growth*, *237*, 383–389.

Waite, W. F., W. J. Winters, and D. H. Mason (2004), Methane hydrate formation in partially water-saturated Ottawa sand, *Am. Mineral.*, *89*, 1202–1207.

Winters, W. J., I. A. Pecher, W. F. Waite, and D. H. Mason (2004), Physical properties and rock physical models of sediments containing natural and laboratory-formed methane gas hydrate, *Am. Mineral.*, *89*, 1221–1227.

F. M. Francisca, Facultad de Ingenieria, Universidad Nacional de Cordoba (CONICET), Av. Vélez Sarsfield 1601, Córdoba 5016, Argentina. (ffrancis@gtwing.efn.uncor.edu)

C. Ruppel, School of Earth and Atmospheric Sciences, Georgia Institute of Technology, 311 Ferst Dr, Atlanta, GA 30332–0340, USA. (cdr@eas.gatech.edu)

J. C. Santamarina and T. S. Yun, School of Civil and Environmental Engineering, Georgia Institute of Technology, 790 Atlantic Dr., NW, Atlanta, GA 30332–0355, USA. (carlos@ce.gatech.edu; taesup.yun@ce.gatech.edu)